Supplementary material for

Proapoptotic activity of JNK-sensitive BH3-only proteins underpins ovarian cancer response to replication checkpoint inhibitors

Annapoorna Venkatachalam, Cristina Correia, Kevin L. Peterson, Xianon Hou,
Paula A. Schneider, Annabella R. Strathman, Karen S. Flatten, Chance C. Sine,
Emily A. Balczewski, Cordelia D. McGehee, Melissa C. Larson,
Laura N. Duffield, X. Wei Meng, Nicole D. Vincelette, Husheng Ding, Ann L. Oberg,
Fergus J. Couch, Elizabeth M. Swisher, Hu Li, S. John Weroha,
and Scott H. Kaufmann

SUPPLEMENTARY METHODS

Apoptosis assays

After treatment for the indicated times, nonadherent and trypsinized adherent cells were combined; sedimented; lysed at 4 °C in a solution consisting of 0.1% (w/v) Triton X-100 and 50 μg/ml propidium iodide in 0.1% (w/v) sodium citrate; and subjected to flow cytometry as previously described to assess DNA fragmentation (1,2). Alternatively, cells were stained with APC-conjugated Annexin V and 0.1 μg/ml propidium iodide in 140 mM NaCl, 2.5 mM $CaCl_2$, and 10 mM HEPES (pH 7.4). Cells (30,000 events) were analyzed using the FL2 channel (excitation: 488 nm; emission: 585/21 nm) of a BD Biosciences FACSCanto II flow cytometer and CellQuest software as described (2,3).

Mitochondrial CMXRos assays

To assess mitochondrial membrane potential (4), nonadherent and trypsinized adherent cells were combined after the indicated treatments; sedimented; and washed with calcium- and magnesium-free Dulbecco's phosphate-buffered saline (PBS); and incubated at 37 degrees with cell viability Ghost Dye 780 (Cytek Biosciences, Fremont, CA). Cells were then washed with PBS containing 5% (v/v) goat serum to remove excess dye, stained with MitoTracker Red CMXRos for 30 mins at 37 °C for 30 min, and subjected to flow cytometry. Cells (30,000 events) were acquired on BD Biosciences FACSCanto II flow cytometer and gated on forward and side-scatter for singlet and live cells using FlowJo software (BecktonDickinson, Franklin Lakes, NJ).

Cell fractionation

After drug treatment, cytosol and mitochondria were isolated as previously described (5). In brief, cells were washed twice with calcium- and magnesium-free Dulbecco's phosphate-buffered saline (PBS), incubated for 20 min in hypotonic buffer [25 mM HEPES (pH 7.5), 5 mM $MgCl_2$, 1 mM EGTA, 1 mM EDTA, 1 mM PMSF, 10 μg/ml pepstatin A, 10 μg/ml leupeptin, 1 mM sodium vanadate, and 20 nM microcystin] and lysed with 50-70 strokes in a tight fitting Dounce homogenizer. Lysates were sedimented at 800 x g for 15 min to remove the nuclei (pellet). The post-nuclear fraction was carefully collected and spun at 4000 x g for 15 min to collect crude mitochondria (pellet) and cytosol (supernatant). The post-mitochondrial supernatant was transferred to a fresh tube and spun twice at 105,000 x g for 1 h. Cytosolic protein was precipitated by adding ice cold TCA to a final concentration of 10% (w/v) and washed with -20 °C acetone. Pellets for all cellular fractions were solubilized and further processed as detailed in **Immunoblotting**.

Immunoblotting

To collect samples for processing, ovarian cancer cell lines treated with the indicated agents in the absence or presence of the broad-spectrum caspase inhibitor Q-VD-OPh at 5 μM were washed once with ice-cold RPMI 1640 with 10 mM HEPES (pH 7.4) or PDX tissue was cut to 1 mm sections and processed. Samples were solubilized in buffered 6 M guanidine hydrochloride under reducing conditions and prepared for electrophoresis as described (6). All loading controls are housekeeping proteins and were chosen based on i) availability of high quality antibodies and ii) insensitivity to caspases in the case of blots from apoptotic cells. Using the standard curves provided by serial dilutions of Ovcar5 cells on each blot, relative protein levels were quantified as previously described (7,8).

Quantitative reverse transcriptase-polymerase chain reaction (qRT-PCR)

qRT-PCR was performed in biological triplicates harvested independently from samples collected for RNA-seq using 100 ng RNA and TaqMan One-Step RT-PCR Master Mix (Applied Biosystems, Carlsbad, CA) per the

supplier's instructions using the indicated probes (9). PCR was performed on an ABI Prism 7900HT Real Time System using a program of 48 °C for 30 min, 95 °C for 10 min, then 40 cycles of 95 °C for 15 sec and 60 °C for 1 min. Data analysis was performed using the following equations: $\Delta C_t = C_t$ (sample)-C_t (endogenous control); $\Delta\Delta C_t = \Delta C_t$(sample)-$\Delta C_t$(untreated); and Fold Change = $2^{-\Delta\Delta Ct}$.

RNA sequencing (RNAseq) and analysis

RNAseq was performed as previously described (9,10). Total RNA was prepared from COV362 and PEO1 cells treated for two days with diluent or 20 nM prexasertib using a Qiagen RNAeasy kit. After RNA sample quality was assessed, an Illumina TruSeq mRNA kit was used to generate cDNA for next-generation sequencing. RNAs were poly-A selected and fragmented, then subjected to reverse transcription with random primers and the final genomic library was analyzed on an Illumina HiSeq 4000. STAR aligner (11) was used for sequence alignment to the UCSC hg38 (human). Gene level counts were obtained using featureCounts v1.4.6 from the subRead package . Differential expression analysis was performed with DESeq2 (12).

PDX establishment

Fresh human tumor tissues from consenting patients with ovarian cancer were collected at the time of primary debulking surgery and coded with a patient heterotransplant (PH) number in accordance with the Mayo Clinic Institutional Review Board and the Health Insurance Portability and Accountability Act regulations (IRB 09-008768). A guarantee that all human subject research at Mayo has been reviewed by the IRB has been given to the U.S. Department of Health and Human Services in a Federal-wide Assurance (FWA00005001) and is guided by the statement of principles outlined in The Belmont Report. An IRB-approved written informed consent form was documented in the electronic medical record of every patient. All animal procedures were approved by the Mayo Clinic Institutional Animal Care and Use Committee, consistent with all policies of the American Veterinary Medical Association.

PDX growth analysis

For PDX growth analysis *in vivo*, linear mixed effects modeling, performed in the SAS PROC MIXED procedure, was used to assess differences between groups. The design is a split-split plot in time with experimental units (EU) PDX (corresponding to amplification status), mouse (corresponding to drug), and mouse-by-time (corresponding to drug-by-time). A random effect for PDX nested within amplification status was used to account for natural variation between PDX models and the correlation between mice from the same PDX. The dependent variable was tumor area on the natural log scale. Independent fixed effect variables were chosen guided by goodness of fit metrics Akaike and Bayesian information criteria (AIC, BIC) to be treatment arm, day (centered), day squared, amplification status, and the 2- and 3-way interactions. Correlation between repeated measurements on the same mouse was modeled using the spatial(power) correlation structure. A single multiple degree of freedom hypothesis test of coincident curves accounting for both the mean and slopes was performed. If significant, then single degree of freedom tests for mean and slope were examined to determine the source of differences. Per PDX analyses were performed as well as described in (13). In per PDX analyses, independent variables were treatment arm, day, and the interaction; an additional polynomial term (day squared) was added in a hierarchical manner for PH063 to accommodate tumor growth trajectory shapes.

SUPPLEMENTARY REFERENCES

1. Nicoletti I, Migliorati G, Pagliacci MC, Grignani F, Riccardi C. A Rapid and Simple Method for Measuring Thymocyte Apoptosis by Propidium Iodide Staining and Flow Cytometry. Journal of Immunological Methods **1991**;139:271-9
2. Mesa RA, Loegering D, Powell HL, Flatten K, Arlander SAH, Dai NT, *et al.* Heat Shock Protein 90 Inhibition Sensitizes Acute Myelogenous Leukemia Cells to Cytarabine. Blood **2005**;106:318-27
3. Martin SJ, Reutelingsperger CP, McGahon AJ, Rader JA, van Schie RC, LaFace DM, *et al.* Early Redistribution of Plasma Membrane Phosphatidylserine is a General Feature of Apoptosis Regardless of the Initiating Stimulus: Inhibition by Overexpression of Bcl-2 and Abl. Journal of Experimental Medicine **1995**;182:1545-56
4. Pan R, Ryan J, Pan D, Wucherpfennig KW, Letai A. Augmenting NK cell-based immunotherapy by targeting mitochondrial apoptosis. Cell **2022**;185:1521-38 e18
5. Dai H, Peterson KL, Flatten KS, Meng XW, Venkatachalam A, Correia C, *et al.* A BAK subdomain that binds mitochondrial lipids selectively and releases cytochrome C. Cell Death Differ **2023**;30:794-808
6. Kaufmann SH. Reutilization of immunoblots after chemiluminescent detection. Analytical biochemistry **2001**;296:283-6
7. Kaufmann SH, Karp JE, Jones RJ, Miller CB, Schneider E, Zwelling LA, *et al.* Topoisomerase II Levels and Drug Sensitivity in Adult Acute Myelogenous Leukemia. Blood **1994**;83:517-30
8. Kaufmann SH, Svingen PA. Immunoblot Analysis and Band Depletion Assays. In: Bjornsti M-A, Osheroff N, editors. Protocols for DNA Topoisomerases: Humana Press; 1998. p 253-68.
9. Hurley RM, McGehee CD, Nesic K, Correia C, Weiskittel TM, Kelly RL, *et al.* Characterization of a RAD51C-Silenced High Grade Serous Ovarian Cancer Model During Development of PARP Inhibitor Resistance. NAR Cancer **2021**;3:zcab028
10. Ding H, Vincelette ND, McGehee CD, Kohorst MA, Koh BD, Venkatachalam A, *et al.* CDK2-Mediated Upregulation of TNFalpha as a Mechanism of Selective Cytotoxicity in Acute Leukemia. Cancer Res **2021**;81:2666-78
11. Dobin A, Davis CA, Schlesinger F, Drenkow J, Zaleski C, Jha S, *et al.* STAR: ultrafast universal RNA-seq aligner. Bioinformatics **2013**;29:15-21
12. Love MI, Huber W, Anders S. Moderated estimation of fold change and dispersion for RNA-seq data with DESeq2. Genome Biol **2014**;15:550
13. Oberg AL, Heinzen EP, Hou X, Al Hilli MM, Hurley RM, Wahner Hendrickson AE, *et al.* Statistical analysis of comparative tumor growth repeated measures experiments in the ovarian cancer patient derived xenograft (PDX) setting. Sci Rep **2021**;11:8076
14. Manning F, Conway A, Doyle S. Differential reactivity of native and recombinant piGST in various assay systems. Biochemical Society Transactions **1995**;23:360S
15. Sanchez ER, Toft DO, Schlesinger MJ, Pratt WB. Evidence that the 90-kDa phosphoprotein associated with the untransformed L-cell glucocorticoid receptor is a murine heat shock protein. J Biol Chem **1985**;260:12398-401
16. Lamarre D, Talbot B, Leduc Y, Muller S, Poirier G. Production and characterization of monoclonal antibodies specific for the functional domains of poly(ADP-ribose) polymerase. Biochem Cell Biol **1986**;64:368-76
17. Kaufmann SH, Desnoyers S, Talbot B, Poirier GG. Proteolytic Cleavage of Poly(ADP-ribose) Polymerase in Human Leukemia Cells Treated with Etoposide and Other Cytotoxic Agents. In: Poirier GG, Moreau P, editors. ADP-Ribosylation Reactions. New York: Springer-Verlag; 1992. p 262-8.
18. Weroha SJ, Becker MA, Enderica-Gonzalez S, Harrington SC, Oberg AL, Maurer MJ, *et al.* Tumorgrafts as in vivo surrogates for women with ovarian cancer. Clin Cancer Res **2014**;20:1288-97
19. Liao Y, Smyth GK, Shi W. featureCounts: an efficient general purpose program for assigning sequence reads to genomic features. Bioinformatics **2014**;30:923-30
20. Gu Z, Eils R, Schlesner M. Complex heatmaps reveal patterns and correlations in multidimensional genomic data. Bioinformatics **2016**;32:2847-9

21. Kanakkanthara A, Hou X, Ekstrom TL, Zanfagnin V, Huehls AM, Kelly RL, *et al.* Repurposing Ceritinib Induces DNA Damage and Enhances PARP Inhibitor Responses in High-Grade Serous Ovarian Carcinoma. Cancer Res **2022**;82:307-19
22. Santiago-O'Farrill JM, Weroha SJ, Hou X, Oberg AL, Heinzen EP, Maurer MJ, *et al.* Poly(adenosine diphosphate ribose) polymerase inhibitors induce autophagy-mediated drug resistance in ovarian cancer cells, xenografts, and patient-derived xenograft models. Cancer **2020**;126:894-907
23. Al Hilli MM, Becker MA, Weroha SJ, Flatten KS, Hurley RM, Harrell MI, *et al.* In vivo anti-tumor activity of the PARP inhibitor niraparib in homologous recombination deficient and proficient ovarian carcinoma. Gynecol Oncol **2016**;143:379-88
24. Eisenhauer EA, Therasse P, Bogaerts J, Schwartz LH, Sargent D, Ford R, *et al.* New response evaluation criteria in solid tumours: revised RECIST guideline (version 1.1). Eur J Cancer **2009**;45:228-47
25. Kaufmann SH, Karp JE, Svingen PA, Krajewski S, Burke PJ, Gore SD. Elevated Expression of the Apoptotic Regulator Mcl-1 at the Time of Leukemic Relapse. Blood **1998**;91:991-1000
26. Domcke S, Sinha R, Levine DA, Sander C, Schultz N. Evaluating cell lines as tumour models by comparison of genomic profiles. Nat Commun **2013**;4:2126
27. Nesic K, Krais JJ, Wang Y, Vandenberg CJ, Patel P, Cai KQ, *et al.* BRCA1 secondary splice-site mutations drive exon-skipping and PARP inhibitor resistance. Mol Cancer **2024**;23:158
28. Zhang K, Erkan EP, Jamalzadeh S, Dai J, Andersson N, Kaipio K, *et al.* Longitudinal single-cell RNA-seq analysis reveals stress-promoted chemoresistance in metastatic ovarian cancer. Sci Adv **2022**;8:eabm1831

SUPPLEMENTARY TABLES

Supplementary Table S1

Reagents Used in This Study

Antibodies		
Antibody	Supplier	Cat # or reference
Actin Antibody (C-11)	Santa Cruz	Cat # sc-1615
ATR Antibody	Cell Signaling Technology	Cat # 13934
Phospho-ATR (Thr^{1989})	Genetex	GTX128145
Monoclonal anti-α-tubulin	MilliporeSigma	Cat # T9026
Anti-BAK (Ab-1) Mouse mAb (TC-100)	Calbiochem	Cat # AM03-100UG
Anti-BAK antibody, NT	Millipore	Cat # 06-536
BAX mAb (6A7)	BD Biosciences	Cat # 556467
BAX antibody	Cell Signaling Technology	Cat # 2772
Anti-BID Rat mAb	Gift from David Huang	N/A
BIM antibody (C34C5)	Cell Signaling Technology	Cat # 2933
BMF antibody (E5U2J)	Cell Signaling Technology	Cat # 50542
B23/NPM1	https://doi.org/10.1016/0014-4827(86)90461-1	
CASP3 antibody	BD Biosciences	Cat # 610323
Cleaved CASP3 (Asp^{175}) (5A1E) Rabbit mAb	Cell Signaling Technology	Cat # 9664
CASP9 antibody	Cell Signaling Technology	Cat # 9502
CDC25A antibody	Abcam	Cat # ab989
Phospho CDC25A antibody	Cell Signaling Technology	Cat #9526
CDK2 antibody (D-12)	Santa Cruz	Cat # sc-6248
Phospho-CDC2/CDK2 (Tyr^{15}) antibody	Cell Signaling Technology	Cat # 9111
CHK1 antibody (G-4)	Santa Cruz	Cat # sc-8408
Phospho-CHK1 (Ser^{296}) (D3O9F) Rabbit mAb	Cell Signaling Technology	Cat # 90178
Phospho-Chk1 (Ser^{317}) (D12H3) XP® Rabbit mAb	Cell Signaling Technology	Cat #12302
c-FOS (9F6) Rabbit mAb	Cell Signaling Technology	Cat # 2250

Phospho-c-FOS (Ser^{32}) (D82C12) XP	Cell Signaling Technology	Cat # 5348
c-JUN (60A8) Rabbit mAb	Cell Signaling Technology	Cat # 9165
Phospho-c-JUN (Ser^{63}) (54B3) Rabbit mAb	Cell Signaling Technology	Cat # 2361
Phospho-c-JUN (Ser^{73}) (D47G9) XP® Rabbit mAb	Cell Signaling Technology	Cat # 3270
FADD	BD Transduction Labs	Cat #610400
GAPDH (14C10) Rabbit mAb	Cell Signaling Technology	Cat # 2118
GSTpi	Biotrin International	(14)
Histone H2A.X antibody	Cell Signaling Technology	Cat # 2595
Anti-phospho-Histone H2A.X (Ser^{139}) mAb,	Active Motif	Cat # 39117
Anti-phospho-Histone H2A.X (Ser^{139}) mAb, clone JBW301	EMD Millipore	Ca # 05-636
HSP90β Antibody (clone H9010)	Gift from David Toft	(15)
Lamin B1 mAb (A-11)	Santa Cruz	Cat # sc-377000
MCL1 antibody	Cell Signaling Technology	Cat # 4572
MRE11 (31H4) Rabbit mAb	Cell Signaling Technology	Cat # 4847
NOXA (PMAIP1) mAb (114C307.1)	Enzo	Cat # ALX-804-408-C100
Phospho-NPM1 (Thr^{199}) antibody	Cell Signaling Technology	Cat #3541
PARP1 (C-2-10) Mouse mAb	Gift from Guy Poirer	(16,17)
Cleaved PARP1 (Asp^{214}) (D64E10)	Cell Signaling Technology	Cat # 5625
PUMA α/β mAb(G-3)	Santa Cruz	Cat # sc-374223
RAD51 antibody	Abcam	Cat # 133534
RAF Antibody	PharMingen	Cat # 554134
RPA32 antibody	Bethyl Laboratories	Cat # A300-244A
Phospho-RPA32 (S^4/S^8) antibody	Bethyl Laboratories	Cat # A300-245A
Phospho-SAPK/JNK (Thr^{183}/Tyr^{185}) antibody	Cell Signaling Technology	Cat # 9251
SAPK/JNK Antibody	Cell Signaling Technology	Cat # 9252
WEE1 antibody	Cell Signaling Technology	Cat # 4936
Oligonucleotides		
siBAK	Ambion	Cat # s531069
siBAX	Ambion	Cat # s1888
siBIM	Ambion	Cat # s531070
siBID	Ambion	Cat# 120774
siBMF	Invitrogen	Cat # s40385
siCDC25A #1	Ambion	Cat # s2751

siCDC25A #2	Ambion	Cat # 121332
siCDC25A pool	Dharmacon	Cat # L00322800
siJNK1 #1	Ambion	Cat # s11152
siJNK1 #2	Ambion	Cat # s11154
siJNK1 pool	Dharamcon	Cat # 5514
siJNK2 #1	Ambion	Cat # 11159
siJNK2 #2	Ambion	Cat # s229708
siJNK2 pool	Dharamcon	Cat # 3505
siNOXA	Ambion	Cat # AS002LFN
siPUMA	Ambion	Cat # AS026N78
Negative Control siRNA	Ambion	Cat # AM4636
BAK- Forward Primer ACG GCA GCT CGC CAT CAT CG	Invitrogen	N/A
BAK-Reverse Primer CGA TGA TGG CGA GCT GCC GT	Invitrogen	N/A
BAX-Forward Primer GCG AGT GTC TCA AGC GCA TC	Invitrogen	N/A
BAX- Reverse Primer GAT GCG CTT GAG ACA CTC GC	Invitrogen	N/A
BID -Forward Primer CGCA GAGA GCTG GACG CACT	Invitrogen	N/A
BID -Reverse Primer AGTG CGTC CAGC TCTC TGCG	Invitrogen	N/A
gRNA targeting FADD GCGGCGCGTCGACGACTTCG	Genscript	N/A
Recombinant DNA		
LentiCrispr V2	Addgene	Cat #52961
Primers for Real-Time PCR		
BIM	ThermoFisher	Cat # Hs00197982-m1
FASLG	ThermoFisher	Cat # Hs00181226-g1
FOS	ThermoFisher	Cat # Hs01119266-g1
GAPDH	Applied Biosystems	Cat # 4352665
JUN	ThermoFisher	Cat # Hs01103582-s1
NOXA	ThermoFisher	Cat # Hs00560402-m1
PUMA	ThermoFisher	Cat # Hs00248075-m1
TNFα	ThermoFisher	Cat # Hs01113624-g1
TRAF1	ThermoFisher	Cat # Hs01090170-m1
TRAIL	ThermoFisher	Cat # Hs00921974-m1

Critical Commercial Assays		
Allophycocyanin (APC) Annexin V	BD Pharminogen	Cat # 550475
SuperSignal West pico PLUS Chemiluminscent Substrate	ThermoFisher	Cat #34580
Lipofectamine 2000 Transfection Reagent	Invitrogen	Cat # 11668030
CellTitre-Glo Luminescent Viability Assay	Promega	Cat # G7570
Tumor Dissociation Kit	Miltenyi Biotec	Cat # 130-096-730
Biological samples		
Patient-derived xenografts (PDXs)	Animal Models Core of the Mayo Clinic Ovarian Cancer SPORE	https://www.mayo.edu/research/centers-programs/cancer-research/research-programs/womens-cancer-program/ovarian-cancer-spore/cores/animal-model-core. (18)
Chemicals, peptides and Recombinant Proteins		
Prexasertib	Chemietek	Cat # 550475
Ceralasertib	AstraZeneca	AZD6738
Adavosertib	AstraZeneca	AZD1775
Olaparib	Chemietek	CT-A2281
LY2208800	Excen Pharma and Tech	
Hoechst 33258	MilliporeSigma	Cat #94403
Human TRAIL	Bio-Techne	Cat #375-TL-010
Deposited Data		
Raw imaging data	This paper	N/A
RNA-seq data	This paper	GSE215340
Software and Algorithms		
Prism9 GraphPad software	N/A	https://www.graphpad.com
STAR aligner (v2.6.0a)	https://github.com/alexdobin/STAR	(11)
featuresCounts v1.4.6		(19)
SAMtools (v1.3)	http://samtools.sourceforge.net/	

RStudio, Bioconductor 3.17 and R packages: ggplot2; DESeq2; Complex heatmap	https://bioconductor.org/packages/release/bioc/html/DESeq2.html https://bioconductor.org/packages/release/bioc/html/ComplexHeatmap.html	(12,20)
Linear mixed effects regression model to model comparative tumor growth.	In house pipeline	(13)
Adobe Creative Cloud	N/A	https://www.adobe.com/creativecloud.html
Cell Lines		
OVCAR5	Gift from Dr. Dominic Scudiero, NCI Frederick	N/A
OVCAR8	Gift from Dr. Dominic Scudiero, NCI Frederick	N/A
IGROV1	Gift from Dr. Ernst Lengyel, University of Chicago, IL	N/A
A2780	Purchased from Fox Chase Cancer Center, Philadelphia, PA	N/A
COV362	Gift of Robert Van Waardenburg, University of Alabama, Birmingham, AL	N/A
OV90	Gift of Robert Van Waardenburg, University of Alabama, Birmingham, AL	N/A
SKOV3	Gift from Dr. Viji Shridhar, Mayo Clinic, Rochester MN	N/A
PEO1	Gift from Dr. Fergus Couch, Mayo Clinic, Rochester, MN	N/A
PEO4	Gift from Dr. Fergus Couch, Mayo Clinic, Rochester, MN	N/A

Supplementary Table S2

Detailed characteristics of all ovarian cancer patient-derived xenografts (PDXs) used for *ex vivo* assessment

PDX ID	Features[a]	MYC copy #	CCNE1 copy #	TP53	HRD score[b]	*BRCA1/2* mutation status	PARPi response[d]	% survival prexasertib[e]	% survival ceralasertib[e]
PH048*	HRDlow, PARPi resistant	5.45	2	TP53 p.S127Y	17	WT	Resistant (21)	ND	64
PH081	HRD low, PARPi resistant	ND[c]	ND	TP53 p.V157F	17	WT	Resistant	66	82
PH026	HRD low, PARPi resistant	4.57	9.54	TP53 p.S127F	22	WT	Resistant	ND	85
PH235	HRD low, PARPi resistant	4.6	9.5	TP53 p.H214fs	29	WT	Resistant	50	83
PH160	HRD high, PARPi sensitive	ND	ND	TP53 p.L93fs	47	WT	Sensitive	81	77
PH061	HRD high, PARPi resistant	3.9	2.0	TP53 p.Y234N	49	BRCA2 p.S3366fs	Resistant	63	60
PH088	HRD high, PARPi sensitive	3.0	2.0	TP53 p.P316fs	49	BRCA1 p.S1253fs	Sensitive	ND	52
PH063*	HRD high, PARPi resistant	2.0	1.2	TP53 p.F109fs	51	WT	Resistant (22)	70	ND
PH233	HRD high, PARPi resistant	ND	ND	TP53 p.P190T	64	WT	Resistant	83	66
PH039*	HRD high, PARPi sensitive	3.89	2.0	TP53 p.N239T	67	WT	Sensitive (21)	38	40
PH127	HRD high	ND	ND	WT	72	BRCA1 p.W1815X	Not tested	14	81
PH013	HRD high, PARPi sensitive	4.2	2.5	TP53 p.T253P	79	WT	Sensitive	74	66
PH345*	HRD high, PARPi sensitive	ND	ND	TP53 p.E51X	ND	WT	Sensitive (21)	96	76
PH354	PARPi resistant	19	24	TP53 p.Y126fs	ND	WT	Resistant	75	67
PH365	PARPi resistant	ND	ND	TP53 p.Y220C	ND	WT	Resistant	73	ND
PH490		ND	ND	WT	ND	WT	Not tested	ND	68
PH538		ND	ND	WT	ND	WT	Not tested	ND	54
PH606		ND	ND	ND	ND	ND	Not tested	48	63

[a]Selected genetic characteristics of PDXs assayed for sensitivity to prexasertib, ceralasertib, and adavosertib *ex vivo*. Underlined PDXs were selected for *in vivo* testing, PDXs in blue are $CCNE^{amp}$ MYC^{amp} models.

[b]HRD score determined by Myriad Genetics MyChoice CDX® test on PDX tissue.

[c]ND – not determined

[d]PARPi response determined by PDX *in vivo* drug testing. *, methods and results from the following models are published (9,23). The remainder will be published in the near future (S.J. Weroha *et al*., in preparation).

[e]% survival after 5 µM prexasertib or 5 µM ceralsertib from *ex vivo* PDX testing.

Supplementary Table S3

Clinical characteristics of patients providing ovarian cancer patient-derived xenografts (PDXs) used for *ex vivo* and *in vivo* assessment

PDX ID (PH)	Gender	Age	Diagnosis	Primary Tissue	Specimen collected	Collection Site	Histology	Grade	Stage	Treatment	Status at last follow-up	Months from diagnosis to last follow-up	Tumor Timepoint
PH048	F	60	Ovarian Carcinoma	Ovary	Ovary	Primary	Serous	High	IIIC	Naïve	Death	2	Primary
PH081	F	82	Ovarian Carcinoma	Ovary	Ovary	Primary	Serous	High	IV	Neoadjuvant	Persistence	14	Primary
PH026	F	68	Primary peritoneal carcinoma	Ovary	Ovary	Primary	Serous	High	IIIC	Naïve	Recurrence	5	Primary
PH235	F	75	Ovarian Carcinoma	Ovary	Ovary	Primary	Serous	High	IIIC	Naïve	Recurrence	19	Recurrent
PH160	F	65	Ovarian Carcinoma	Ovary	Ovary	Primary	Serous	High	IIIC	Naïve	Death	148	Primary
PH061	F	75	Ovarian Carcinoma	Ovary	Ovary	Primary	Serous	High	IIIC	Naïve	Death	14	Primary
PH088	F	45	Ovarian Carcinoma	Ovary	Ovary	Primary	Serous	High	IIIC	Naïve	Recurrence	20	Recurrent
PH063	F	63	Ovarian Carcinoma	Ovary	Ovary	Primary	Serous	High	IIIC	Naïve	No event	159	Primary
PH233	F	57	Ovarian Carcinoma	Ovary	Ovary	Primary	Serous	High	IIIC	Naïve	Recurrence	13	Primary
PH039	F	62	Fallopian Tube Carcinoma	Fallopian Tube	Fallopian Tube	Primary	Serous	High	IIIC	Naïve	Recurrence	22	Primary
PH127	F	58	Ovarian Carcinoma	Ovary	Ovary	Primary	Serous	High	IIIC	Naïve	Recurrence	22	Primary
PH013	F	71	Ovarian Carcinoma	Ovary	Ovary	Primary	Serous	High	IIA	Naïve	No event	165	Primary
PH345	F	57	Ovarian Carcinoma	Ovary	Ovary	Primary	Serous	High	IIIC	Naïve	Recurrence	122	Primary
PH354	F	60	Ovarian Carcinoma	Ovary	Omentum	Omentum	Serous	High	IIIC	Neoadjuvant	Recurrence	12	Primary

PH365	F	73	Ovarian Carcinoma	Ovary	Ovary	Primary	Serous	High	IIIC	Naïve	Recurrence	22	Primary
PH490	F	81	Ovarian Carcinoma	Ovary	Ovary	Primary	Serous	High	IIIC	Naïve	Recurrence	66	Primary
PH538	F	68	Ovarian Carcinoma	Ovary	Ovary	Primary	Serous	High	IIIC	Naïve	Recurrence	51	Primary
PH606	F	66	Ovarian Carcinoma	Ovary	Ovary	Primary	Serous	High	IVB	Naïve	Recurrence	21	Primary

Supplementary Table S4

Survival outcomes in PDXs

Ref=Control

outcome		HR	CI.lower.HR	CI.upper.HR	p.value	p.value.wald
OS:PH061	**AZD1775 (80 mg/kg)**	29972669.93	0.00	Inf	0.998	0.054
	AZD6738 (35 mg/kg)	269853405.46	0.00	Inf	0.998	
	Olaparib (50 mg/kg)	120878883.41	0.00	Inf	0.998	
OS:PH063	**AZD1775 (80 mg/kg)**	1.29	0.47	3.49	0.622	0.102
	AZD6738 (35 mg/kg)	1.03	0.37	2.87	0.958	
	Olaparib (50 mg/kg)	0.32	0.09	1.13	0.076	
OS:PH235	**AZD1775 (80 mg/kg)**	0.51	0.18	1.44	0.206	0.198
	AZD6738 (35 mg/kg)	1.36	0.50	3.65	0.546	
	Olaparib (50 mg/kg)	1.38	0.52	3.65	0.516	
OS:PH354	**AZD1775 (80 mg/kg)**	0.23	0.05	1.08	0.063	0.101
	AZD6738 (35 mg/kg)	0.72	0.18	2.82	0.638	
	Olaparib (50 mg/kg)	0.19	0.02	1.74	0.143	
PD:PH061	**AZD1775 (80 mg/kg)**	0.05	0.01	0.29	< 0.001	0.009
	AZD6738 (35 mg/kg)	0.58	0.19	1.79	0.339	
	Olaparib (50 mg/kg)	0.56	0.16	2.04	0.382	
PD:PH063	**AZD1775 (80 mg/kg)**	0.68	0.31	1.51	0.345	0.650
	AZD6738 (35 mg/kg)	1.07	0.47	2.45	0.864	
	Olaparib (50 mg/kg)	0.76	0.32	1.80	0.533	
PD:PH235	**AZD1775 (80 mg/kg)**	0.28	0.10	0.76	0.012	0.037
	AZD6738 (35 mg/kg)	0.93	0.39	2.22	0.864	
	Olaparib (50 mg/kg)	0.84	0.34	2.07	0.712	
PD:PH354	**AZD1775 (80 mg/kg)**	0.00	0.00	Inf	0.996	0.351
	AZD6738 (35 mg/kg)	0.49	0.20	1.20	0.119	
	Olaparib (50 mg/kg)	0.51	0.22	1.18	0.114	
PFS:PH061	**AZD1775 (80 mg/kg)**	0.10	0.02	0.45	0.003	0.003
	AZD6738 (35 mg/kg)	1.08	0.38	3.05	0.889	
	Olaparib (50 mg/kg)	0.59	0.17	2.09	0.414	
PFS:PH063	**AZD1775 (80 mg/kg)**	0.68	0.31	1.51	0.345	0.650
	AZD6738 (35 mg/kg)	1.07	0.47	2.45	0.864	
	Olaparib (50 mg/kg)	0.76	0.32	1.80	0.533	
PFS:PH235	**AZD1775 (80 mg/kg)**	0.32	0.12	0.84	0.021	0.066
	AZD6738 (35 mg/kg)	0.91	0.38	2.18	0.837	
	Olaparib (50 mg/kg)	0.78	0.31	1.93	0.589	
PFS:PH354	**AZD1775 (80 mg/kg)**	0.01	0.00	0.10	< 0.001	< 0.001
	AZD6738 (35 mg/kg)	0.46	0.20	1.10	0.080	
	Olaparib (50 mg/kg)	0.46	0.20	1.05	0.064	

Progressive disease was defined as ultrasound measurement with a 1.44-fold increase in tumor area by transabdominal ultrasound [equivalent to a 20% increase in length dimension used clinically in the RECIST criteria for tumor assessment (24)]. For each PDX, a Cox proportional hazards regression model was used to estimate hazards ratios (HRs), and Wald p-values were used to test the significance of the difference between treatment arms.

SUPPLEMENTARY FIGURES

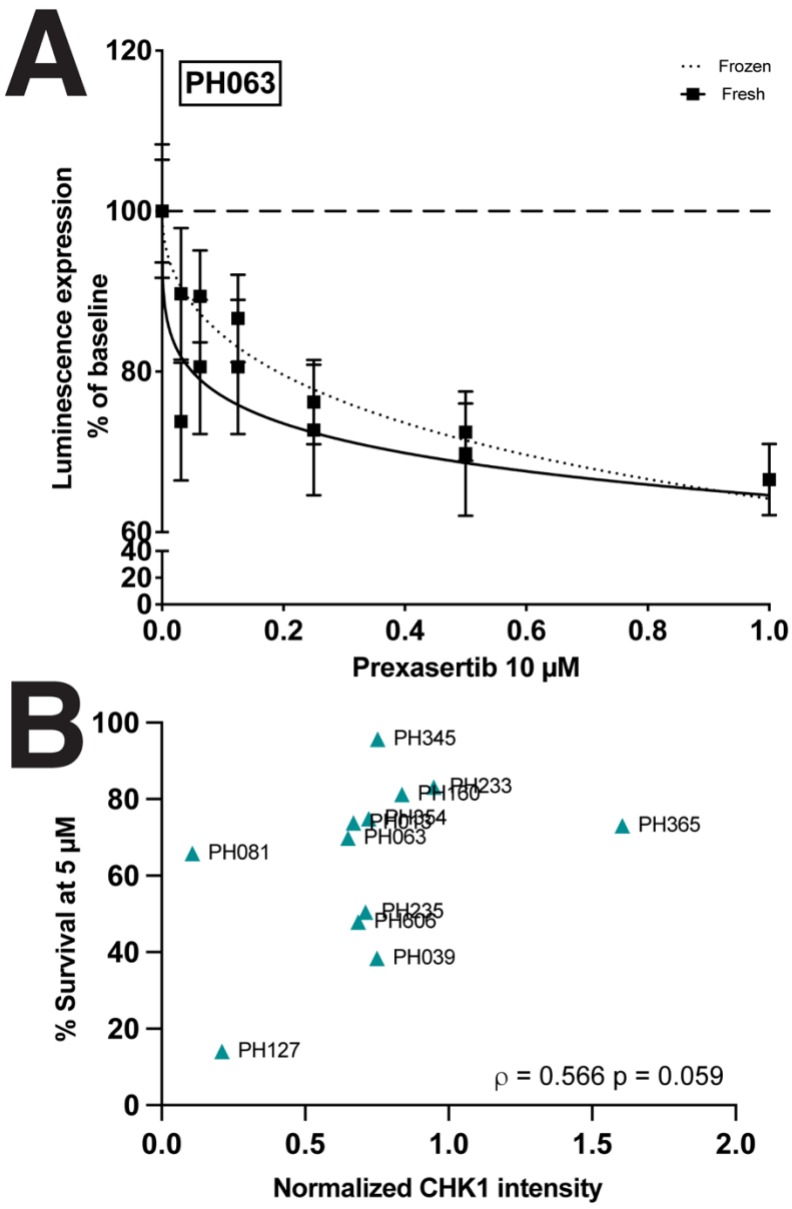

Supplementary Figure S1. CHK1 levels correlate with *ex vivo* PDX sensitivity to prexasertib A, Comparison of fresh and frozen PDX PH063 exposed *ex vivo* to increasing concentrations of prexasertib for three days and assayed for viable cell mass using CellTiter-Glo. **B**, Association of % tumor cell survival and CHK1 levels in PDX assayed *ex vivo* for response to prexasertib using Spearman correlation ($\rho = 0.566$, $p = 0.059$).

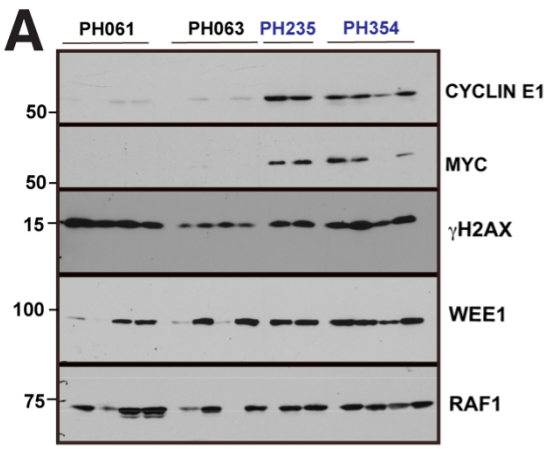

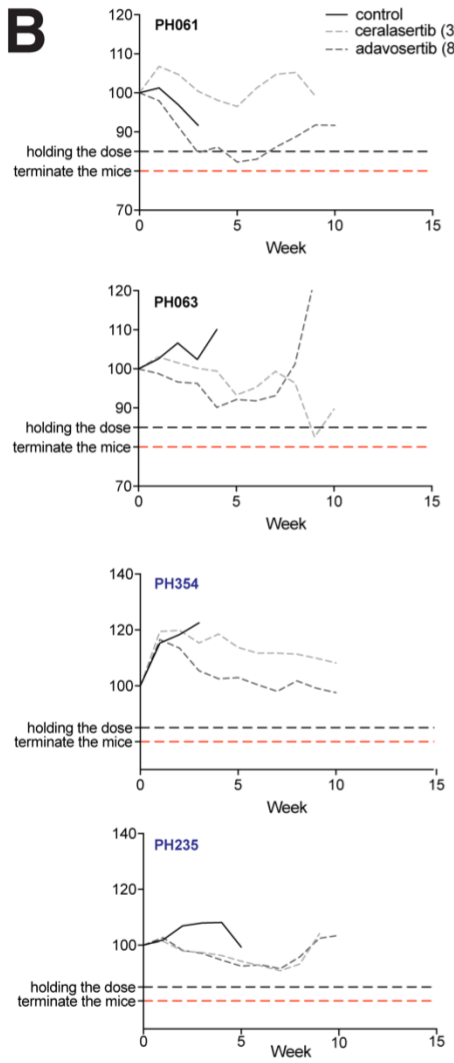

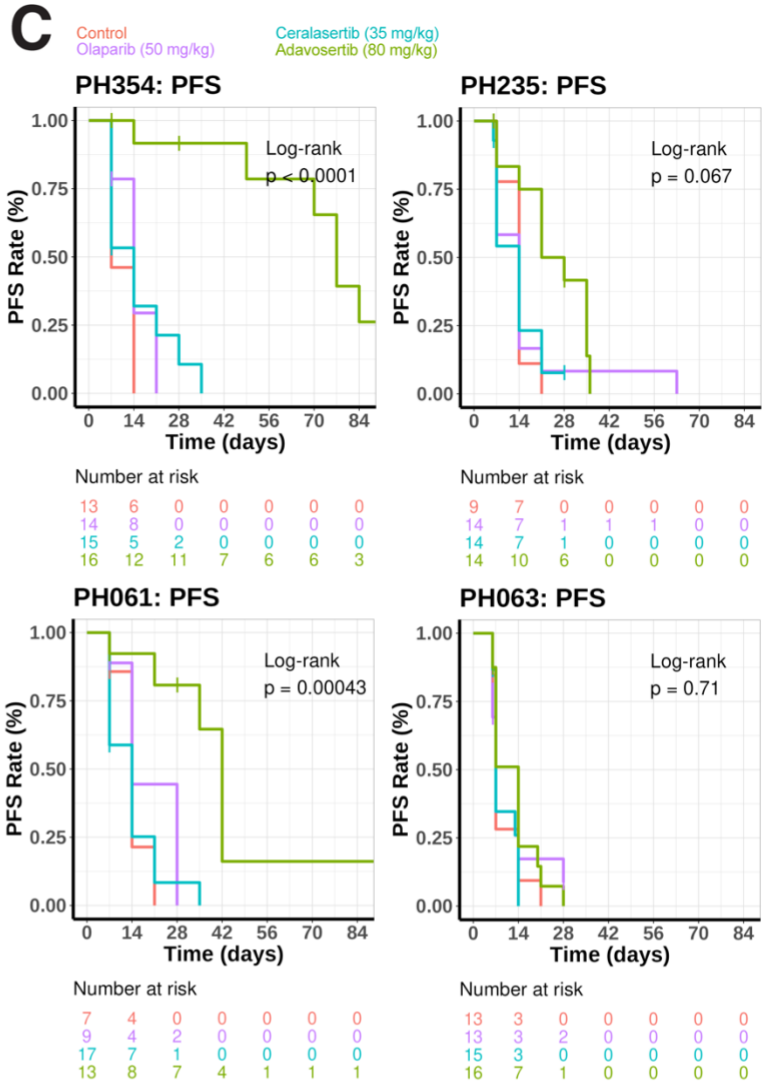

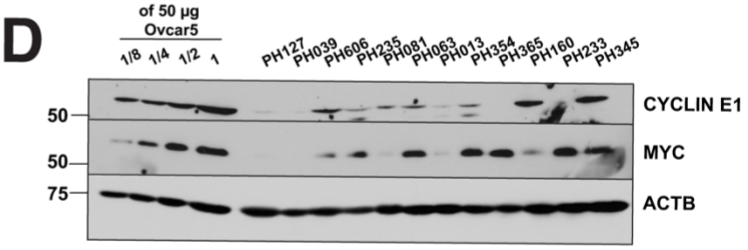

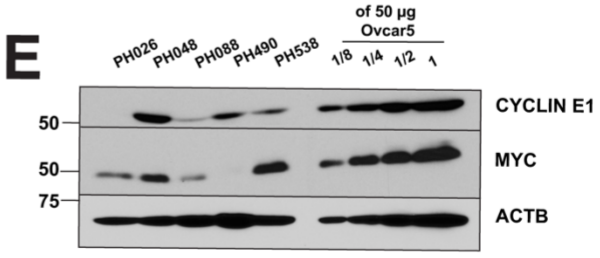

F

Spearman r	Prexasertib % survival at 5 µM	Ceralsertib % survival at 5 µM	Adavosertib % survival at 5 µM
CHK1	0.5664	-0.5429 *	-0.4
WEE1	-0.1189	-0.2571	0.1143
MYC	0.7273 **	0.1036	-0.06786
CCNE	0.3427	-0.1429	-0.02143

Supplementary Figure. S2. PDX intrinsic factors and treatment outcomes in HGSOCs treated with replication checkpoint modulators. A, Two to four *in vivo* replicates of untreated PDXs from separate tumored animals were blotted for CCNE1, MYC, and phosphorylated H2AX. The models that are $CCNE^{amp}$ Myc^{amp} are denoted by blue font. The housekeeping protein RAF1 served as a loading control. **B**, Normalized body weights of mice bearing the indicated PDX models in response to vehicle control (solid black line), single agent ceralasertib (light gray dashed line) or adavosertib (dark grey dashed line). Body weight was normalized to pretreatment values and depicted as percent of Day 0. Treatments were withheld if body weight loss was ≥15% of starting weight and mice were euthanized if weight loss was ≥20% of starting weight. **C**, Kaplan-Meier analysis of progression-free survival (PFS) defined as time from treatment initiation (Day 0) to detection of progressive disease, animal death or unplanned sacrifice between treatment arms. Log-rank test was used to test the significance of difference between treatment arms. **D**, CCNE and MYC levels across ovarian carcinoma PDX models (ordered by % survival at 5 μM to prexasertib, with most sensitive on the left), with serial dilutions of Ovcar5 cells as a standard curve to permit quantitation of blots (8,25). **E**, CCNE and MYC in PDXs that were tested for sensitivity to ceralasertib and adavosertib but not prexasertib, (ordered by % survival at 5 μM to ceralasertib, with most sensitive on the right). **F**, Association of CHK1, WEE, MYC, and CCNE levels in PDX assayed *ex vivo* for response to prexasertib, ceralasertib, and adavosertib using Spearman correlation.

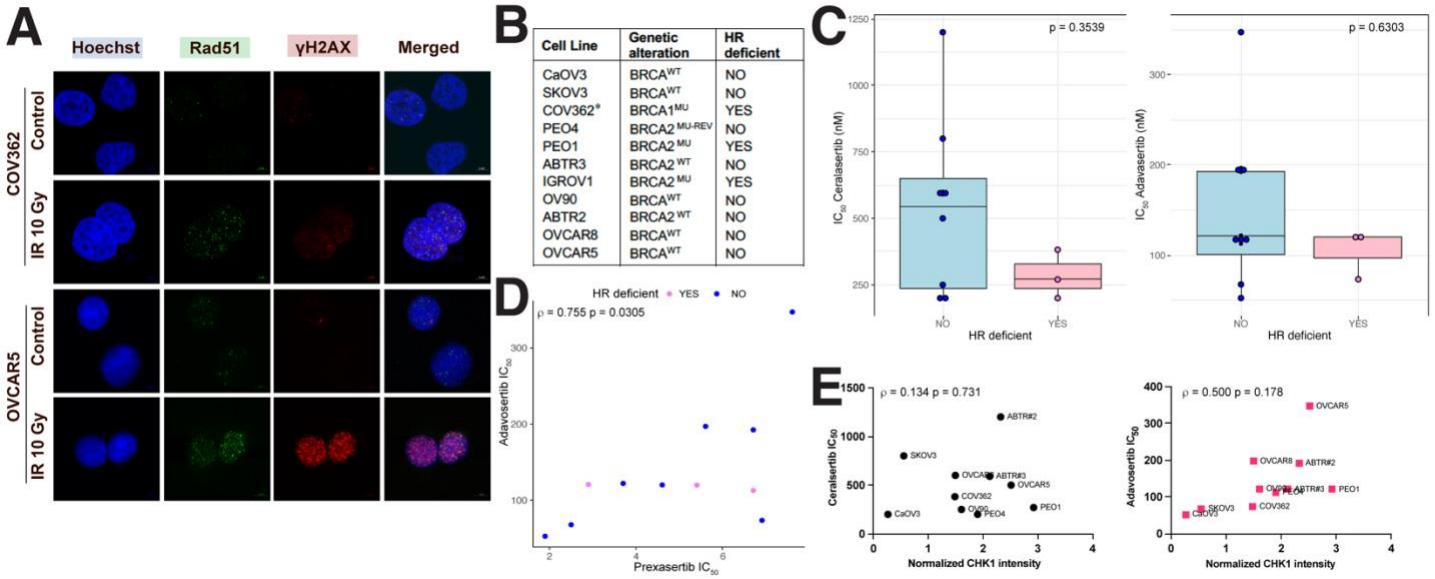

Supplementary Figure. S3. Analysis of HGSOC cell line intrinsic factors to RCM response. A, To define HR status, cells were subjected to 10 Gy ionizing radiation, incubated for 6 h, fixed, co-stained for nuclear RAD51 and γH2AX, and imaged (100 cells/treatment). Scale bar = 5 μM. **B**, Summary of genetic alterations and functional HR status as indicated by IR-induced RAD51 nuclear foci in ovarian cancer cell lines. Cell lines are ordered as in Fig. 3B. * indicates the presence of *MYC* amplification (26). Formation of weak RAD51 foci in COV362 despite the homozygous BRCA1 nonsense mutation has been previously reported and attributed to low level expression of a hypomorphic exon 11-skipping splice variant (27). **C**, Assessment of association between HR deficiency and IC_{50} to ceralasertib (left) or adavosertib (right) using Wilcoxon rank sum test. P = 0.3539 and 0.6303, respectively. **D**, Scatter plot showing correlation between prexasertib IC_{50} and adavosertib IC_{50} by HR status ($\rho = 0.755$, p= 0.0305). **E**, Association between ceralasertib IC_{50} (left) or adavosertib IC_{50} (right) and CHK1 levels using Spearman correlation.

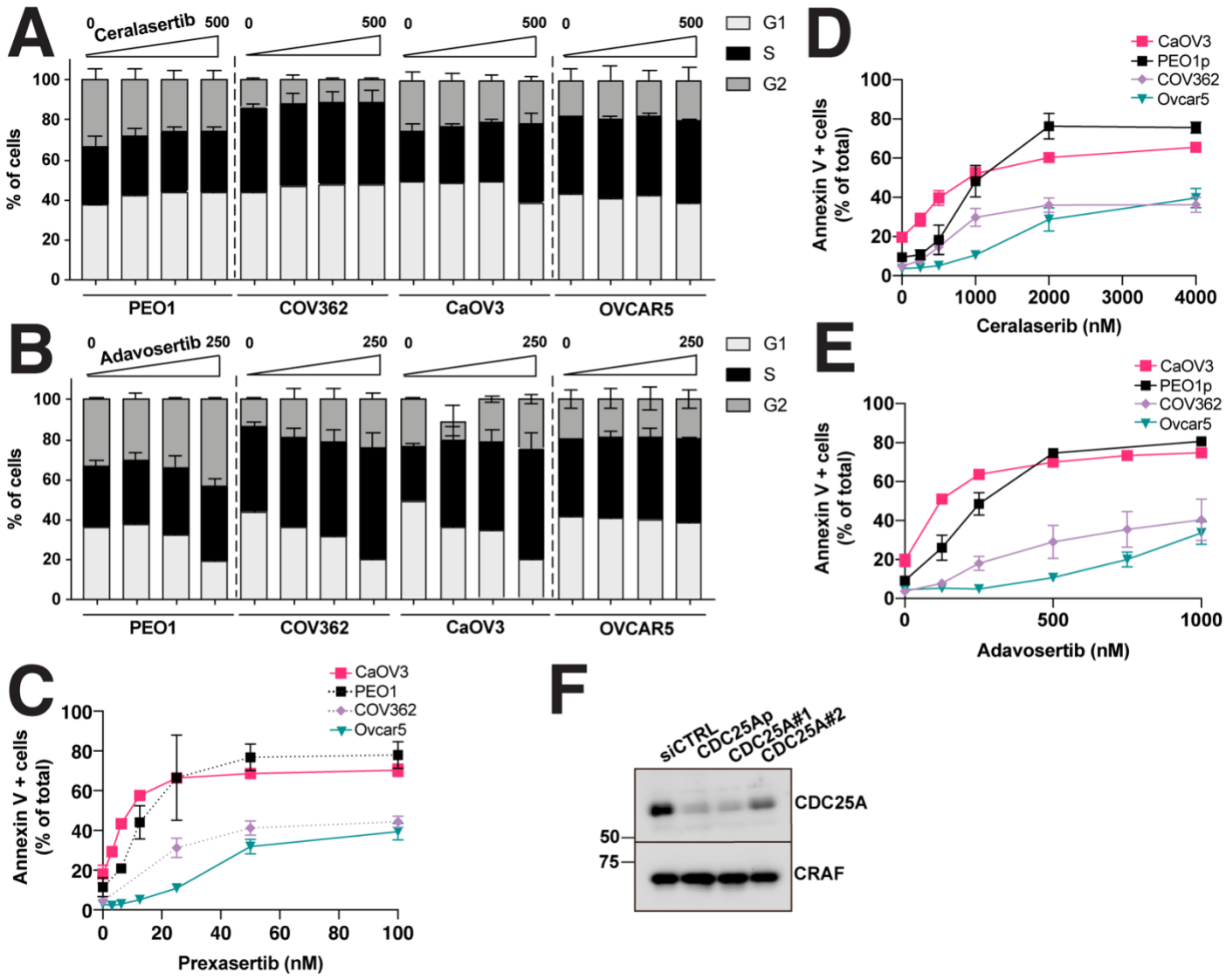

Supplementary Figure S4. ***In vitro*** **characterization of HGSOC cell lines to RCM therapy. A, B,** PEO1, COV362, CaOV3, and OVCAR5 cells, were treated with increasing concentrations of ceralasertib (A) or adavosertib (B) for 24 h, stained with propidium iodide and analyzed by flow cytometry. Error bars indicate mean ± SEM for mean of three independent experiments. **C-E**, Ovarian cancer cell lines CaOV3, parental (p) COV362, PEO1, and OVCAR5 were treated for five days continuously with prexasertib (C), ceralasertib (D), or adavosertib (E) and analyzed for Annexin V+ cells by flow cytometry. Error bars, mean ± SEM for mean of three independent experiments. Dashed lines indicate the results shown in Figure 2E. **F**, Extracts from PEO1 cells transfected with indicated single siRNAs (#1, #2) and siRNA pool to CDC25A (CDC25Ap) or negative control as described in Figure 2F were immunoblotted with the indicated antibodies.

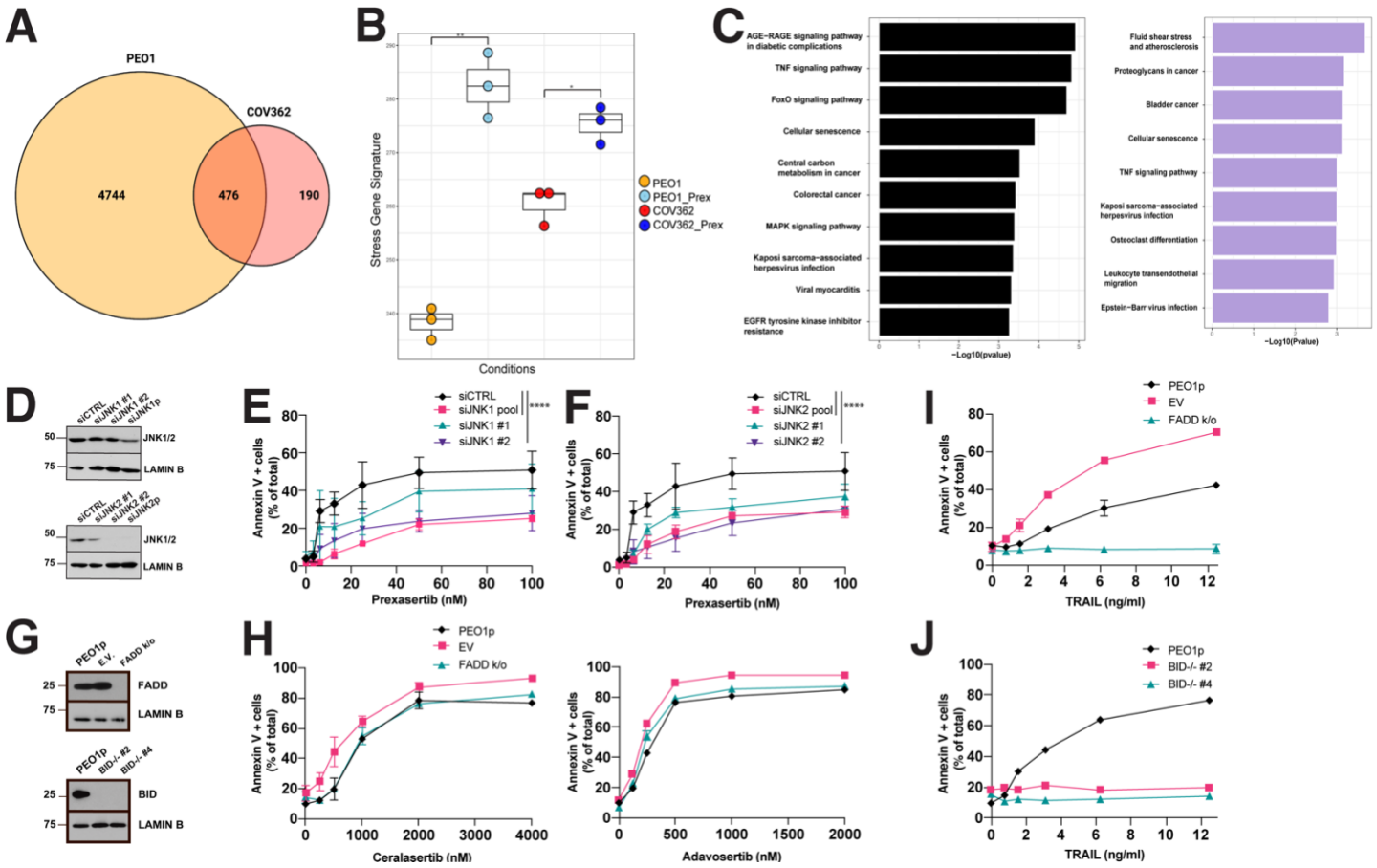

Supplementary Figure S5. c-JUN kinase and stress-activated pathway in RCM cytotoxicity. A, Venn diagram showing common differentially expressed genes between PEO1 and COV362 ovarian cancer cell lines treated with 20 nM prexasertib. **B**, Stress signature in diluent- vs prexasertib-treated samples. Data are represented as the total expression of stress genes in biological replicates and the number of asterisks indicates statistical significance by t-test for paired samples with equal variance (28). **C**, KEGG enrichment analysis for differential genes detected in both PEO1 and COV362 cell lines treated with prexasertib ($p < 0.05$, n= 750 for PEO1; n = 666 for COV362). **D**, Immunoblots to assess JNK levels in PEO1 cells transfected with indicated single siRNAs or pooled siRNAs. **E, F**, PEO1 cells treated with siRNAs to JNK1 (E) or JNK2 (F) followed by five days of prexasertib exposure were assayed for Annexin V binding. Error bars, mean ± SEM for three independent experiments. siJNK1pool (siJNK1p), siJNK1 and siJNK1 single siRNA #1 (siJNK-s1) vs siCTRL, ****p <0.0001; siJNK2p, siJNK2-s1 vs siCTRL, ****p <0.0001 using two-way ANOVA with Dunnett's multiple comparisons test. **G**, Immunoblots to assess FADD (top) and BID (bottom) levels in the indicated PEO1 cell populations. **H**, Parental PEO1 (PEO1p) populations stably transduced with sgRNA targeting FADD or empty vector (EV) were treated for five days with increasing concentrations of ceralasertib or adavosertib and assayed for Annexin V binding. Error bars, mean ± SEM from three independent experiments. **I, J**, Pooled PEO1 cells transduced with empty vector (EV), FADD sgRNA (I), or BID knockout clones (J) were treated for 24 h with increasing concentrations of recombinant human TRAIL and assayed for Annexin V binding. Error bars, mean ± SEM for three independent experiments.

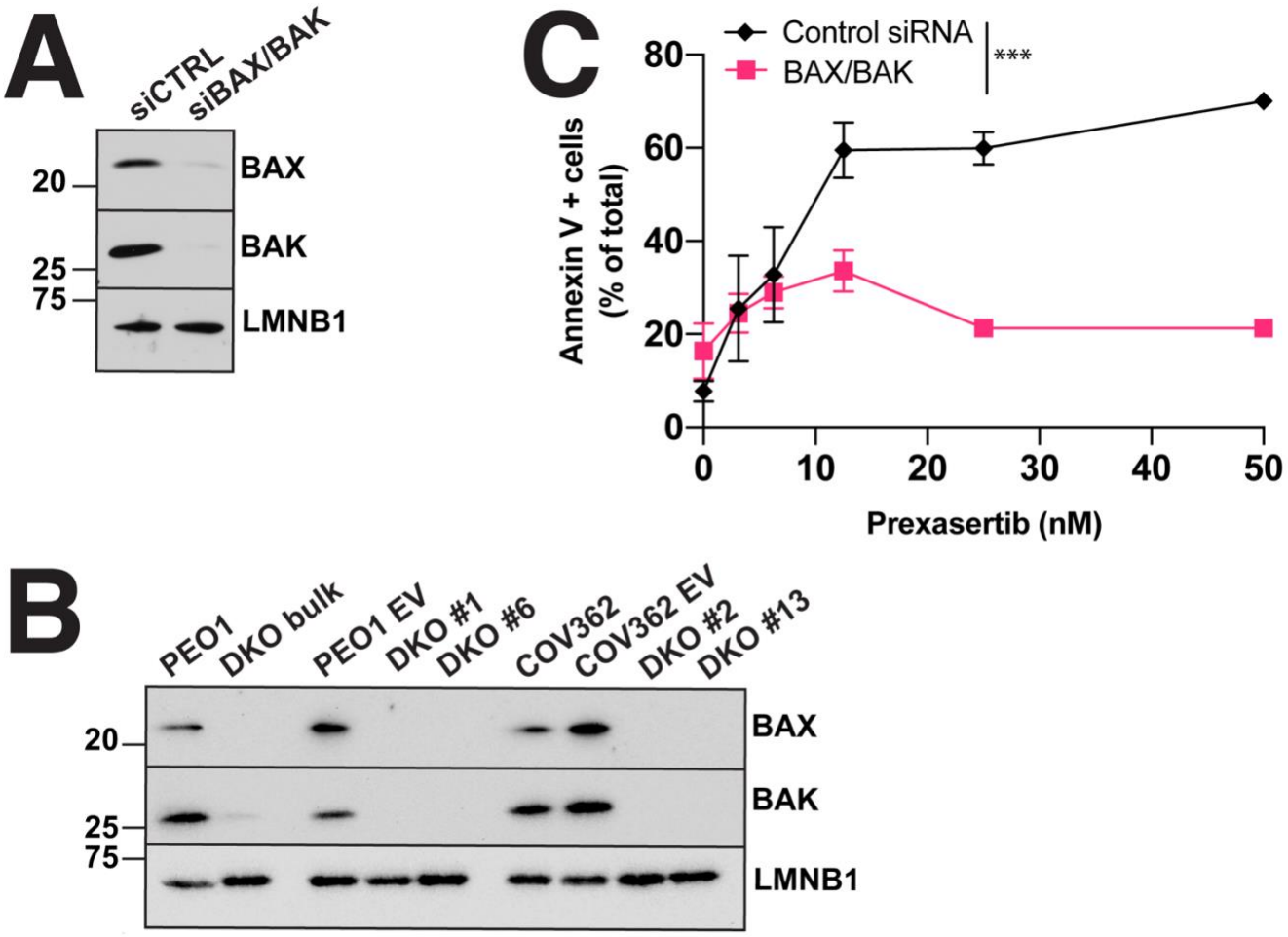

Supplementary Figure S6. BAX and BAK contribute to RCM cytotoxicity. A, Immunoblots to assess BAX and BAK levels in PEO1 cells transfected with siRNAs to BAX and BAK. **B**, Immunoblots to assess BAX and BAK interruption in the indicated PEO1 and COV362 clones. **C**, Annexin V+ cells in PEO1 cells treated with indicated siRNA to BAX and BAK, followed by prexasertib treatment for five days. Error bars, mean ± SEM for three or more independent experiments. siBAX/BAK vs siCTRL, ***$p < 0.001$ using two-way ANOVA with Dunnett's test for multiple comparisons.

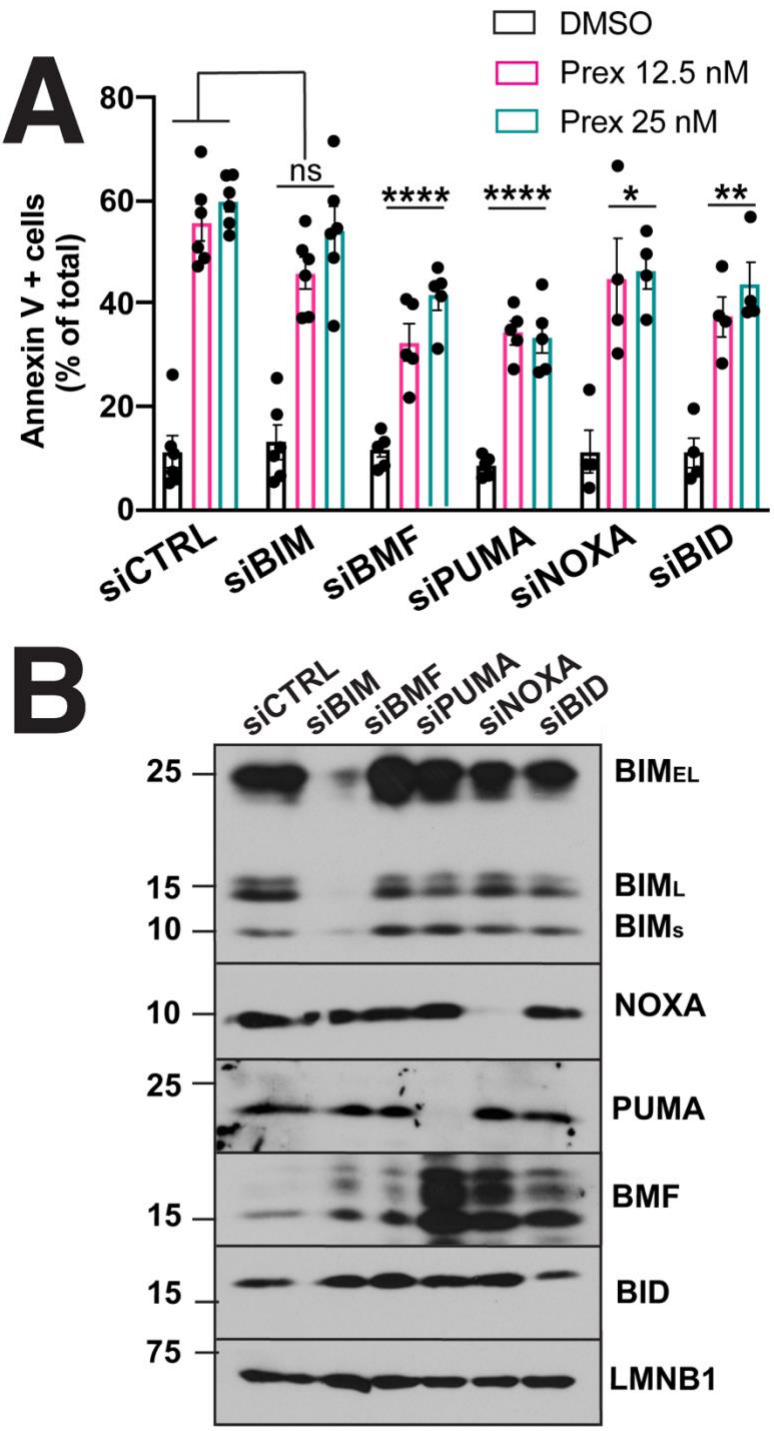

Supplementary Figure 7. Role of BH3 proteins in RCM-induced cytotoxicity A, PEO1 cells were treated with the indicated siRNAs, exposed to prexasertib for five days, and stained with Annexin V. Error bars, ± SEM for three or more independent experiments. siNOXA vs siCTRL, *$p < 0.05$; siBID vs siCTRL, **$p < 0.01$; siBMF vs. control and siPUMA vs siCTRL, ****$p < 0.0001$ using two-way ANOVA with Dunnett's test for multiple comparisons. **B**, Immunoblots to assess BH3-protein levels in PEO1 cells transfected with the indicated individual siRNAs.